Proceedings Paper:

Terzioglu, F. orcid.org/0000-0002-2639-2992, Rongong, J., Odavic, M. et al. (2 more authors) (2025) Integrity of power electronic components on a rotating PCB. In: Proceedings of the International Exhibition and Conference for Power Electronics, Intelligent Motion, Renewable Energy and Energy Management (PCIM Europe 2025). International Exhibition and Conference for Power Electronics, Intelligent Motion, Renewable Energy and Energy Management (PCIM 2025), 06-08 May 2025, Nuremberg, Germany. VDE Publishing House ISBN 9783800765416

Integrity of Power Electronic Components on a Rotating PCB

Furkan Terzioglu[1], Jem Rongong[1], Milijana Odavic[1], Hemanth V. Betha[1], Kais Atallah[1]
[1] University of Sheffield, UK

Corresponding author: Milijana Odavic, m.odavic@sheffield.ac.uk
Speaker: Milijana Odavic, m.odavic@sheffield.ac.uk

Abstract

This paper presents an initial study on the physical integrity of small power electronic components mounted on a rotating Printed Circuit Board (PCB) using solder-pin pairs. A practical approach, based on measured failure stress of the solder-pin pairs, is used to predict the rotational speeds – and corresponding inertial forces – at which components may lose their connection to the PCB. High-speed rotational tests of the PCB are conducted to validate the approach. Results indicate that the method provides conservative predictions for the failure of inertial loads of the components, ensuring a safety factor in practical applications.

1 Introduction

As electrically driven machines become increasingly common in engineering applications, the integration of power electronics on rotating drives along with their accommodating PCB has a great potential in various fields. However, this introduces physical design challenges related to the reliable operation of power electronics [1] although the employment of potting materials [2], [3] would offer a practical solution to reduce the effect of rotation.

When a PCB rotates, inertial forces are generated on the power electronic components, proportional to their masses in directions perpendicular to the rotational axis. These forces create bending moments at the points where pin-solder pairs are connected to the PCB, leading to high stress levels and potential operational failures.

This work aims to investigate the durability of small power electronic components (e.g., capacitors, transformers) mounted on a rotating PCB and provide a pre-guide to the designer seeking to model a safe operation for a rotating PCB with a range of power electronics. A series of theoretical and experimental analyses was conducted to assess the operational integrity of these components under significant rotation-induced loading.

2 Stress Analysis of a PCB Exposing Inertial Loads

When the PCB rotates at a specified rotational speed, the inertial loads are generated on the small electronic components shown in Fig.1. These loads produce bending moments on the PCB locations at which the pin-solder couplings are attached to the PCB. This can result in high stress levels on the locations where the pin-solder couplings are attached to the PCB and could lead to operational failures of the small electronic components. This section presents the numerical estimations for these stress levels by conducting static FEM simulations of the PCB and the influence of a potting fill that can be placed between the PCB and the casing to reduce these stress levels. Note that the static analysis only requires evaluating the stiffness matrix of a spatially-discretised structure along with the boundary conditions (including external forces).

2.1 Numerical Model

A numerical model of the PCB shown in Fig. 1 including the casing and small electronic components was obtained by meshing all parts via ANSYS [4]. The model involved the standard quadratic element types of the package software, and the total number of nodes employed in the model was 375150. The model was fixed by the bottom inner edges. A constant rotational speed of 125 rad/s was applied to all parts of the model to compute the corresponding inertial forces due to the rotation included in the FEM model as the external forces.

The model was formed by different parts: PCB, casing, mini board, capacitors, small capacitors, transformer, pins and solder joints. To simplify the model, capacitors, small capacitors and transformers were modelled as point masses supposing that these parts were much stiffer than the other parts. All parts were considered to be independent from each other in the model. This meant that each part had a different stiffness matrix. Therefore, the global stiffness matrix and the equations of the static simulations were constructed implementing an interaction method between the parts. Each part had also individual material properties in the model as shown in Table 1.

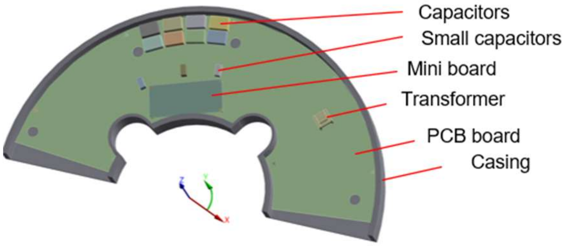

Fig. 1 A PCB geometry with various small electronic components in a casing

Name	Elastic modulus [GPa]	Mass [kg]
Casing	69	5.400
PCB board	21.6	0.250
Mini board	21.6	0.050
Solders – each	31.5	0.081e-3
Pins – each	110	0.033e-3
Bolts – each	69	0.315e-3 – 0.564e-3
Nuts – each	69	0.053e-3
Small capacitors – each	-	0.004
Capacitors – each	-	0.031
Transformer	-	0.030

Table 1 Material properties used for each part of the PCB model

2.2 Experimental Characterisation of a Typical Potting Compound

The elastic modulus of a typical potting material for filling the cavities between the PCB and the casing was experimentally studied in this section to report potential changes in the elastic modulus of the potting material with different conditions. The material was a flame retardant thermally conductive epoxy resin. This study can show the reliable operating conditions of the potting material considered to use and indicate the specifications of a reliable potting material required.

Fig. 2 demonstrates the DMA machine (the compression mode was used) used to measure the elastic modulus of the potting material. Under the specified dynamic amplitude, temperature and frequency, the DMA machine measures the complex stiffness of a cylindrical sample (k*) produced from the material whose properties are aimed to be determined. The details about both how the complex stiffness of a sample is obtained and how samples are placed in the machine can be found in the user-manual of the machine [5].

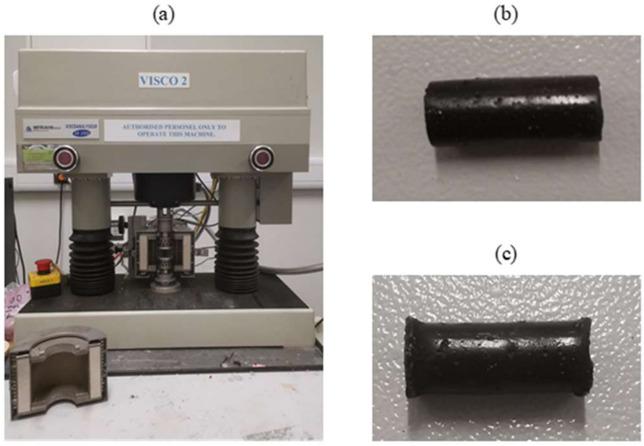

Fig. 2 Pictures of the modulus testing: (a) DMA machine used, (b) a cylindrical sample before testing, (c) a cylindrical sample after testing

The elastic modulus is determined from the complex stiffness of the sample tested by using the length (L) and cross-section area (A) of the cylindrical sample as shown below.

$$E = \mathrm{real}(k^*)L/A \quad (1)$$

For the testing, three cylindrical samples (see Fig. 2b for an example) were prepared by applying the mixing and curing processes provided on the material datasheet. To ensure the reliability, the samples was left to cure for three days (more than the 48 hours suggested on the sheet) before testing. The dimensions and weights of these samples are listed in Table 2.

Each sample was tested by applying a pre-compression (0.1% static strain) to limit the free motions of the samples. There were three main measurement types that were followed for a sample in the testing procedure. The first one was to study the modulus of a sample for varying dynamic strain at a specific frequency whilst the temperature was approximately kept the same. In the second measurement type, the modulus of a sample was tested for a range of frequency by providing both the same dynamic strain and approximately the same temperature. In the last investigation, the modulus of a sample was tested by changing the temperature of the sample using an environmental chamber around the sample placed.

Property	Sample 1	Sample 2	Sample 3
Diameter [mm]	8.50	8.50	8.50
Length [mm]	21.10	22.30	19.25
Weight [g]	1.39	1.47	1.27
Density [kg/m^3]	1160.93	1161.68	1162.64

Table 2 Dimensions and weights of the samples tested

The measurements of each sample are set out in Fig. 3. The results show that the elastic modulus is consistently just below 1 GPa for 10 Hz and 20 Hz excitation, and it is nearly insensitive to the dynamic strain amplitude. Fig. 3b demonstrates that an increase in the frequency results in higher elastic modulus – from just above 100 MPa to just above 1 GPa for an increase from 1 Hz to 100 Hz. The elastic modulus of this potting material significantly changes with the temperature as shown in Fig. 3c. It is just below 1 GPa for a room temperature and sharply decreases to about 0.1 MPa at 80°.

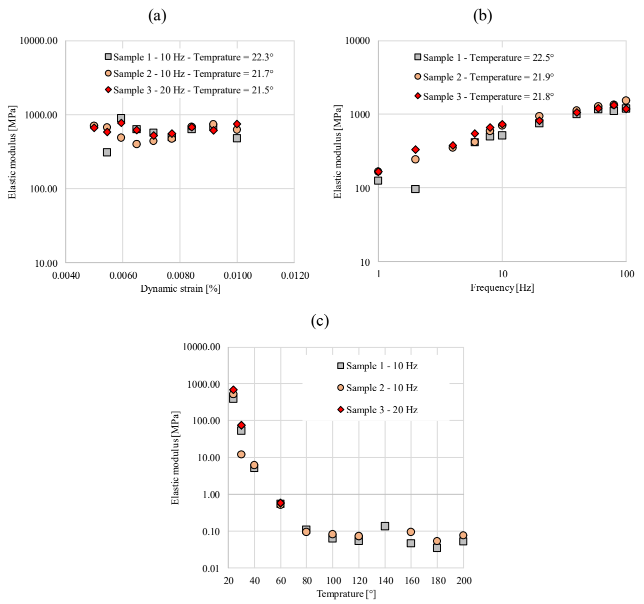

Fig. 3 Elastic modulus of the epoxy material tested as a function of: (a) dynamic strain, (b) frequency, and (c) temperature

2.3 PCB Stress Results

The stress fields of the PCB that was obtained by running a static simulation of the FEM model is presented Fig. 4.

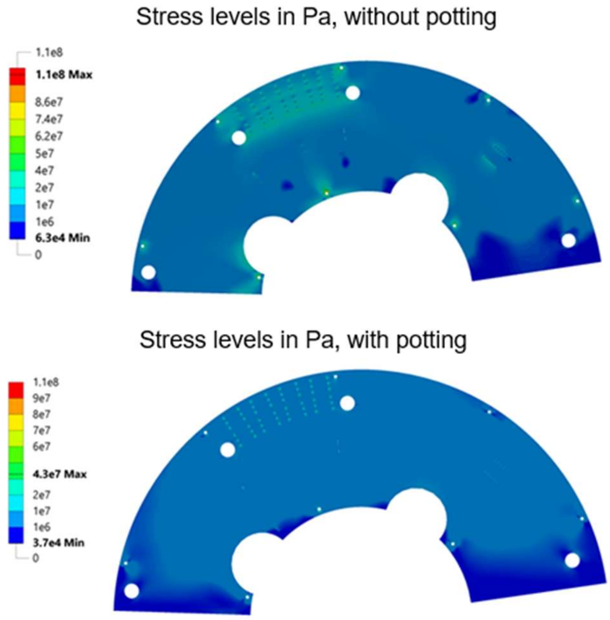

Fig. 4 Resulting stress fields in PCB

Without a potting compound, the maximum stress observed in the solution is about 110 MPa around a bolt hole whilst the average across the PCB is 10.6 MPa. The typical solution for reducing the maximum and overall stress levels of a PCB is the deployment of a potting compound that fills the cavities between the PCB and the casing. To evaluate the effect of a potting compound-fill on the PCB, the PCB model was simulated by adding two layers of potting compound to the model. The density of the potting compound used was set to the average of those shown in Table 2. The elastic modulus ranged between 1 MPa and 10 GPa for a comprehensive investigation and, the Poisson's ratio was selected as 0.41 in the simulations. The stress field of the PCB with the potting compound which has 400 MPa elastic modulus is also shown in Fig. 4 for comparison. It clearly indicates the reduction in the stress levels across the PCB.

To quantify the level of this stress reduction, the relative changes in the maximum and average stresses are demonstrated in Fig. 5 as a function of the elastic modulus of the potting compound. It shows that both maximum and average stress of the PCB are higher than the case without potting case for very low elastic modulus values – see 1 MPa results in the figure. These stress levels decrease with increasing elastic modulus. The reductions reach 50%-60% with 100 MPa elastic modulus. The results indicate that the reductions in the maximum and average stresses does not considerably change for an elastic modulus larger than 100 MPa. This can be related to the elastic modulus of the PCB. As a general conclusion, it can be said that if the use of a potting compound is planned, the selection of the potting compound material should be performed considering the sensitivity of its modulus to operating conditions.

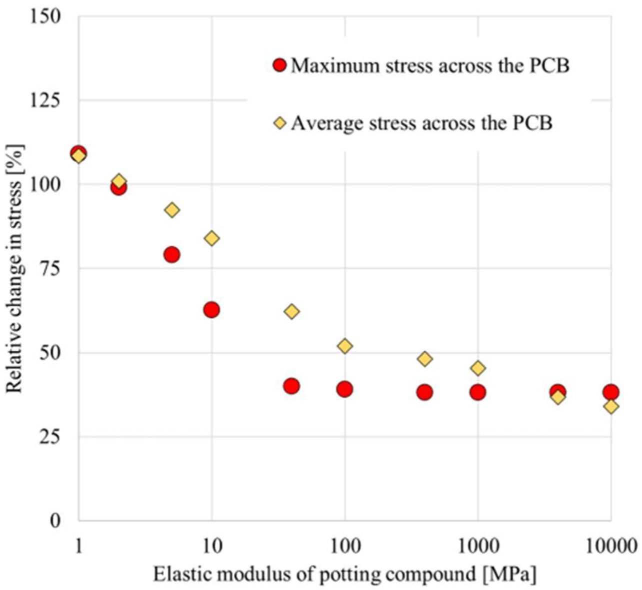

Fig. 5 Changes in the maximum and average stress across the PCB with the elastic modulus of the potting compound used

The stress analysis conducted shows that the high stress occurs around the locations where the bolts and the pin-solder coupling are connected to the PCB. Since the bolts and casing typically have a much higher load capacity than the pin-solder couplings, potential failures are more likely to occur in the pin-solder connections, indicating a need for a detailed investigation.

3 Estimating Failure Inertial Load

The high stress localisation observed in PCB results from the bending force acting on each pin by the rotating small electronic components. Thus, based on the bending behaviour of pins, this section presents a simple prediction methodology for the maximum inertial load that a small electronic component can be exposed before one of its pins loses physical integrity with the PCB.

3.1 Determination of the Pin Tensile Failure Load

To predict the maximum inertial loads under which small electronic components can safely operate, the first step is to determine the tensile failure load of the pins. To determine the tensile failure load of pin-solder pairs on the PCB, a pull test was conducted on a series of samples, as shown in Fig. 6. One end of a pin is connected to the electronic component and the other end of the pin is attached to the PCB by soldering them to each other.

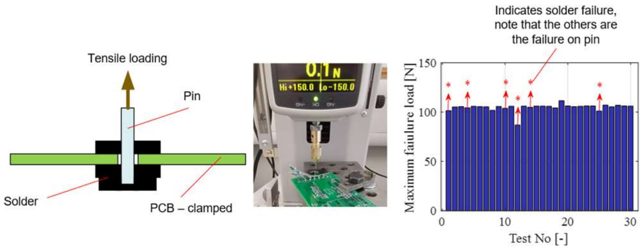

Fig. 6 Testing of tensile failure load for the connection between solder-pin pairs and PCB

The typical diameter of the pins used in the measurements was 0.8 mm. Note that this is one of the most commonly used pin diameters for PCB connections. The material of pins and solders were a copper alloy whose yield stress and UTS were about 250 MPa and 400 MPa respectively according to the typical properties given in technical datasheets. An IMADA mechanical force-displacement machine with a built-in force transducer (having 500 N limit) was used for the measurements. The largest force observed in each force-displacement measurement was identified as the failure tensile load.

Two distinct failure mechanisms were observed: pin breakage and the disintegration of the pin-solder pair caused by the pin tip slipping from its soldered connection. The minimum and maximum stresses at the failure loads were found to be about 100 MPa and 200 MPa. The highest stress observed was smaller than the corresponding UTS and yield stress of the material used. This showed that there was either a weakness in both pin-capacitor and pin-solder connections or stress concentration on the body of pins as a result of geometric inconsistencies.

3.2 Prediction of the Pin Bending Failure Load

Using the results of the tensile testing, the bending behaviour of pins due to the rotation-based inertial loads of small electronic components can be estimated. This can generate a design guide for the safe operation of small electronic components while the PCB rotates at a constant speed.

Supposing that the radial deformations of the PCB are small compared to the bending deflections of the electronic components, a simple model can be considered as shown in Fig. 7. This model simulates a single pin as a cantilever beam with one end fixed to the PCB and subjected to a transverse inertial force at the tip due to rotation.

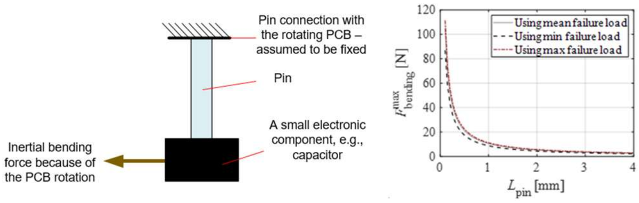

Fig. 7 Failure inertial load model for a pin and failure force behaviour as a function of pin length

Assuming that the pin is under pure bending, the maximum bending force that the pin can carry is:

$$F^{max}_{bending} = \left(F_{tensile,failure} / A_{pin,failure}\right) I_{pin} / \left(L_{pin} d_{pin} / 2\right) \quad (2)$$

where $F_{tensile,failure}$ is the tensile failure force of the pin obtained in the tensile tests, $A_{tensile,failure}$ is the cross-section area of the pin failed in the tensile tests, I_{pin} is the second moment of the cross-section area of the pin that carries the electronic component, L_{pin} is the effective length of the pin that carries the electronic component, d_{pin} is the diameter of the pin that carries the electronic component.

The bending failure load of a pin is shown in Fig.7 as a function of the effective pin length considering 0.8 mm pin diameter. This indicates that the pin bending failure load significantly increases if the effective pin length decreases. The mean, minimum and maximum tensile failure loads obtained in the tensile tests are considered when creating the graph to show the potential effect of changes because of the uncertainty in the measurement of the tensile failure load. It is apparent from the figure that this uncertainty is less important than the effective pin length.

It is clear that Equation 2 determines the limiting bending force for a pin. When the PCB rotates at a constant speed of ω_{PCB}, the bending force acting on one of the pins that carry a small electronic component considered can be calculated as:

$$F_{bending} = m_{component} \omega_{PCB}^{2} r_{component} / n_{component} \quad (3)$$

where $m_{component}$ is the mass of the small electronic component considered (e.g., a capacitor), $r_{component}$ is the distance of the small electronic component to the rotating axis, $n_{component}$ is the number of the pins that is used to carry the small electronic component.

4 Experimental Testing of PCB at High Rotational Speeds and Validation of the Prediction Method

As shown in Fig. 8, a PCB (as a half of an annular disk) with a range of small electronic components attached on it was used for the integrity tests of small electronic components whilst the PCB was subjected to various rotational speeds. It should be noted that two half disks were produced for the tests to provide a balanced system on the rotating shaft connected to the rotating machine. As can be seen in Fig. 8, these two half PCBs were attached to an aluminum disk. The aluminum disk was fixed to the steel shaft. The shaft (connected to the rotating machine) provided the rotational speed aimed to the PCBs. The mass of the aluminum disk was 0.5 kg and the mass of the rotating shaft was 1 kg. The mass of a PCB (without small electronic components) was 0.28 kg.

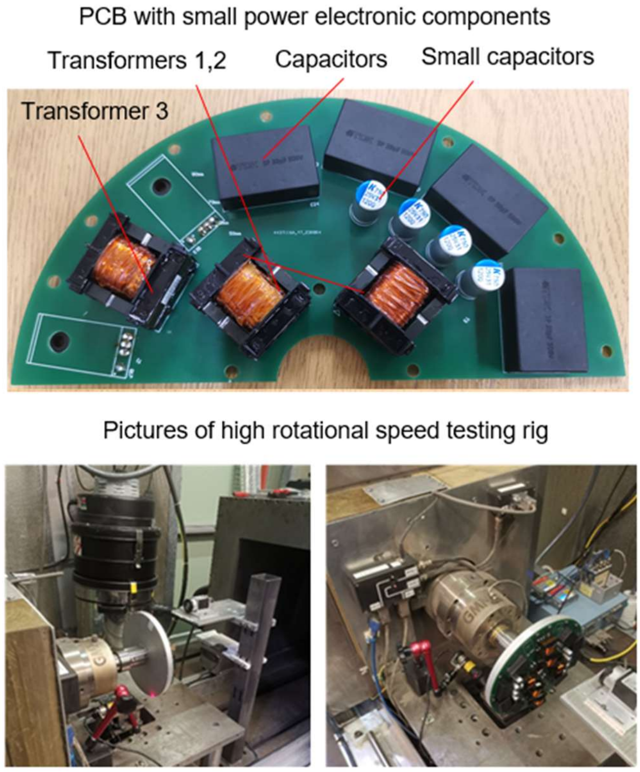

Fig. 8 Tested PCB and test rig for the rotational testing

Transformers, capacitors and small capacitors were the small electronic components for this investigation. The properties of these components can be found in Table 3. These were used to calculate the inertial force on a pin that carries a component.

Component	Component mass [g]	Component distance to rotating centre [mm]	Number of pins used to connect component to PCB[-]	Pin diameter [mm]	Distance between component bottom to PCB [mm]	Effective pin length [mm]
Capacitors	31	75	6	0.8	0.5	0.3
Small capacitors	4.3	60	2	0.6	0.4	0.2
Transformer 1,2	30	35	10	0.8	5	0.4
Transformer 3	30	70	10	0.8	5	0.4

Table 3 Properties of some small electronic components attached to the PCB

As shown in Fig. 8, the PCB assembly was attached to the rotating machine. The rotational speed of the PCB was controlled by a laser probe pointed onto the aluminum disk surface. During the tests, the integrity of small electronic components was checked by both simple electrical property checks conducted regularly (by dividing the whole testing to several batches) and observing the real-time accelerometer signal located on the rotating machine bearing.

During the tests, no electrical capability failure was detected in the components tested. The physical failures of a capacitor and a transformer (they flew away from the PCB and created a spike in the acceleration signal observed) were encountered in the tests. These failures are shown in Fig. 9.

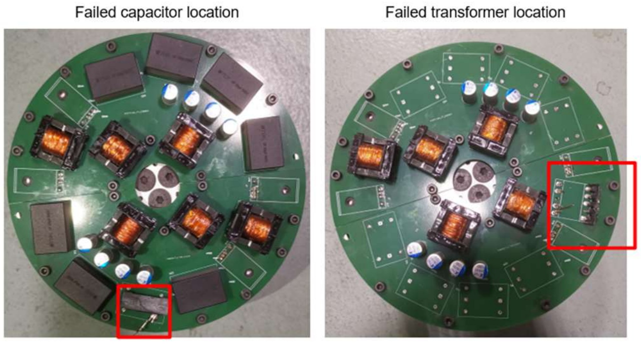

Fig. 9 Failed components

The failure load results and corresponding predictions are shown in Fig. 10.

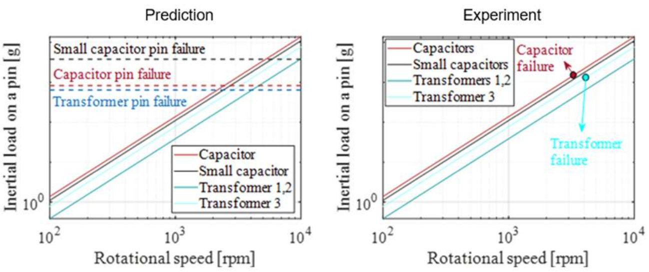

Fig. 10 Comparison of predicted and measured failure inertial loads

The failure of the capacitor was at 3250 rpm at which one of its pins was under 1400g of inertial load. The location of the failed capacitor can be seen from Fig. 9. For the failure of another small electronic component, the PCB needed to rotate at higher speeds than 3250 rpm. To provide a balanced structure for these tests, the other capacitors were removed from the PCB.

The failure speed of the transformer was found to be 4100 rpm at which one of its pins was under 1290g of inertial load. The location of the failed transformer can also be seen from Fig. 9. Note that the tests were terminated at this point as the speed was too much to continue. Therefore, it is clear that the failure of small capacitors is larger than 4100 rpm.

By using the methodology outlined in this paper, the pin failure load was predicted. It was assumed in the prediction method that the pin failure causes the loss of overall component integrity interested. The average tensile failure stress of the pins measured (152 MPa) was used in the failure predictions. To calculate the failure inertial load predictions, the effective pin length estimation is important as it significantly affects the predictions. Table 3 shows the effective pin lengths estimated for each small electronic component. These estimations were obtained by removing the pin length covered by solder or any other physical residuals around the pins from the distance measured between the component interested and the PCB surface.

A comparison of predicted and measured failure loads shown in Fig. 10 indicates that the predicted failure speeds and inertial loads are nearly 50% lower than those measured in the tests. Thus, it is apparent that the prediction method presented in this paper provides a conservative estimation of the failures (with about a safety factor of 2). This difference can arise from several causes. Major reasons are listed below:

I) uncertainty and error in estimating the effective pin length,

II) stress concentration on the pins used in the pin tensile strength measurements,

III) errors in the measurement of pin and component properties.

5 Conclusions

- When the PCB is operational (rotating at a constant speed), the PCB regions, where pins and bolts are attached to the PCB, have been found the most critical in terms of stress due to rotational-induced inertial loads.
- Observed stress levels on the PCB can be reduced about 60% by using a sufficient potting compound (whose elastic modulus should be at least 100 MPa) filled across both sides of the PCB.
- As the temperature is an important parameter for the operation of the electronic components on the PCB, the selection of the potting material should be conducted carefully by determining its modulus characteristic depending on various operational conditions via controlled experiments (such as DMA used in this deliverable report).
- Controlled rotational experiments of the PCB (without any potting compound) has shown that the physical failure of all electronical components

can be encountered at inertial loads larger than 1000g.

- The pin failure prediction method presented in this deliverable report has provided conservative predictions for the electronical components investigated in the controlled rotational experiments.

References

[1] J. K. Nøland and M. Molinas, "Rotating Power Electronics for Electrical Machines and Drives - Design Considerations and Examples," Proc. 15th IEEE Conference on Industrial Electronics and Applications ICIEA 2020, pp. 663-668, Nov. 2020.

doi: 10.1109/ICIEA48937.2020.9248237.

[2] S.A. Meguid, C. Zhuo and F. Yang, "Effective Mitigation of Shock Loads in Embedded Electronic Packaging Using Bilayered Potting Materials." ASME Journal of Electronic Packaging,136(4): 041010. Dec. 2014.

https://doi.org/10.1115/1.4026542.

[3] L. E. Reinhardt, J. A. Cordes, A. S. Haynes, and J. D. Metz, (April 19, 2013). "Assessment of Need for Solder in Modeling Potted Electronics During Gun-Shot", ASME Journal of Applied Mechanics, 80(3): 031502, May 2013. https://doi.org/10.1115/1.4023336.

[4] Ansys 2022 R2, Academic Research Mechanical, 2022.

[5] MetraVib, Dynamic Mechanical Analyzers User Manual, n.d. www.01db-metravib.com.

Acknowledgment

This work is funded through the Clean Sky 2 Joint Undertaking (JU); i.e., the project JTI-CS2-2019-CfP10-LPA-01-77.

Disclaimer

This work reflects only the authors' views, and the JU is not responsible for any use that may be made of the information it contains.